Exploring the Energy Landscape for Q A − to Q B Electron Transfer in Bacterial Photosynthetic Reaction Centers: Effect of Substrate Position and Tail Length on the Conformational G…

4 AUTHORS, INCLUDING:

Laura Baciou

French National Centre for Scientific Research

44 PUBLICATIONS **889** CITATIONS

SEE PROFILE

Pierre Sebban

Université Paris-Sud 11

77 PUBLICATIONS **1,525** CITATIONS

SEE PROFILE

Marilyn R Gunner

City College of New York

72 PUBLICATIONS **4,312** CITATIONS

SEE PROFILE

Exploring the Energy Landscape for Q_A^- to Q_B Electron Transfer in Bacterial Photosynthetic Reaction Centers: Effect of Substrate Position and Tail Length on the Conformational Gating Step[†]

Qiang Xu,[‡] Laura Baciou,[§] Pierre Sebban,[§] and M. R. Gunner*,[‡]

Department of Physics, City College of New York, 138th Street and Convent Avenue, New York, New York 10031, and Centre de Génétique Moléculaire, CNRS, Gif/Yvette, France

ABSTRACT: The ability to initiate reactions with a flash of light and to monitor reactions over a wide temperature range allows detailed analysis of reaction mechanisms in photosynthetic reaction centers (RCs) of purple bacteria. In this protein, the electron transfer from the reduced primary quinone (Q_A^-) to the secondary quinone (Q_B) is rate-limited by conformational changes rather than electron tunneling. Q_B movement from a distal to a proximal site has been proposed to be the rate-limiting change. The importance of quinone motion was examined by shortening the Q_B tail from 50 to 5 carbons. No change in rate was found from 100 to 300 K. The temperature dependence of the rate was also measured in three L209 proline mutants. Under conditions where Q_B is in the distal site in wild-type RCs, it is trapped in the proximal site in the Tyr L209 mutant [Kuglstatter, A., et al. (2001) *Biochemistry 40*, 4253−4260]. The electron transfer slows at low temperature for all three mutants as it does in wild-type protein, indicating that conformational changes still limit the reaction rate. Thus, Q_B movement is unlikely to be the sole, rate-limiting conformational gating step. The temperature dependence of the reaction in the L209 mutants differs somewhat from wild-type RCs. Entropy−enthalpy compensation reduces the difference in rates and free energy changes at room temperature.

Reactions in proteins generally require structural changes as the reactant passes the transition state to go on to product. It is difficult to follow these changes for a number of reasons. The motions can be too small to be seen in any but the highest resolution structures (*1, 2*), for nonphotoactive proteins it is difficult to synchronize reactions (*3*), and it is hard to trap proteins in identifiable substates for analysis (*4*). The photosynthetic reaction centers (RCs)[1] from purple bacteria have proved to be a useful model system, allowing synchronized single-turnover reactions that can be analyzed to study factors that control the electron- and proton-transfer processes in proteins (*5−7*).

The light reaction of bacterial photosynthesis takes place in RCs embedded in the cell membrane. The absorption of a photon by the electron donor, a bacteriochrolophyll dimer (P), triggers a series of electron transfers between bound cofactors, creating a separation of charge across the protein.

P is oxidized (P^+) and first the primary quinone (Q_A) and then the secondary quinone (Q_B) reduced. The ≈100 μs electron transfer from Q_A^- to Q_B is rate-limited by a conformational change in isolated RCs from *Rhodobacter sphaeroides* with native ubiquinone as Q_A and Q_B (*8, 9*).

As a result of the needed conformational changes, the electron transfer from Q_A^- to Q_B shows significant activation enthalpy. If RCs are frozen in the dark, in the ground state, the reaction slows so it cannot be seen as the temperature is lowered. However, RCs frozen under illumination in the product $P^+Q_B^-$ state return to the ground state trapped in a different conformation. Now electron transfer from Q_A^- to Q_B occurs even below 40 K with high yield (*10, 11*). Analysis of the temperature dependence of the reaction has begun to reveal a number of substates and the thermodynamic differences and barriers between these states (*11−13*).

In dark-adapted RCs at physiological pH (6−8) keeping the room temperature, little proton uptake accompanies electron transfer from Q_A^- to Q_B. Previous measurements (*13*) have shown the reaction free energy change ($\Delta G°_{AB}$) is −90 meV with favorable $\Delta H°_{AB}$ (−230 meV) and unfavorable $T\Delta S°_{AB}$ (−140 meV) [pH 8, 298 K, 66% glycerol (v/v)]. There is a barrier to electron transfer of ≈500 meV which is mostly $\Delta H^{‡}_{AB}$ (420 meV). Additional substates of the reactant, $P^+Q_A^-$, have been identified. For example, at low pH the reaction freezes out more slowly than predicted, showing the presence of an active state ≈40 meV above the inactive, dark-adapted state (*13*). Measurements at high pH have characterized an unprotonated reactant

---

* To whom correspondence should be addressed. Telephone: 212-650-5557. Fax: 212-650-6940. E-mail: gunner@sci.ccny.cuny.edu.
[‡] City College of New York.
[§] Centre de Génétique Moléculaire, CNRS.
[1] Abbreviations: RCs, reaction centers; P, bacteriochlorophyll dimer which is the primary electron donor; Q_A and Q_B, primary and secondary quinone electron acceptors; $P^+Q_A^-$ and $P^+Q_B^-$, reactant ($P^+Q_A^-Q_B$) and product ($P^+Q_AQ_B^-$) redox states, respectively. All equilibrium and rate constants have a two-letter subscript. The first is the reactant and the second the product substate. K_{AB} and k_{AB} are the effective equilibrium and rate constants between all subpopulations of $P^+Q_A^-$ and $P^+Q_B^-$ under the conditions of measurement.

substate and measured the barrier to proton uptake (*13*). Thus, experiments on wild-type RCs provide a quantitative picture of the energy landscape connecting $P^+Q_A^-$ and $P^+Q_B^-$. However, alone they provide little information about the atomic nature of the changes whose barriers are being measured.

A variety of conformational changes have been proposed as the rate-determining step for the electron transfer. Q_B is found in several positions in a binding channel in both *Rhodobacter sphaeroides* (*14, 15*) and *Rhodopseudomonas viridis* (*16*) RCs. In the crystal structure of RCs frozen under illumination trapped in an active state, Q_B is both 2.7 Å closer to Q_A than in protein frozen in the dark and flipped by 180° around the tail. Quinone motion from the outer, distal to inner, proximal site has been proposed to be the conformational gating step (*14, 16*). Other studies suggest that shifts of internal protons or changes in the hydrogen bonding pattern may also play a role (*11, 17−19*). Thus, a number of motions may be required for electron transfer. These may contribute to a concerted barrier or pose a number of different hills, any one of which may be rate-determining under different conditions(*13*).

It is possible to explore different barriers to electron transfer by changing protein and substrate. UQ-10 has a 10 unit isoprene tail with 50 carbons. If quinone motion is rate-determining, a shorter tail might be easier to move. Kinetics measured at room temperature show no significant dependence on the quinone tail length (*20, 21*). However, the rate-limiting step might be a protein breathing motion or quinone release from the distal site instead of pure diffusion in the binding channel (*8*). The viscosity increase at low temperature may reveal more dependence on quinone structure if diffusion becomes rate-limiting.

Several water channels leading to Q_B have been identified by structural studies (*14, 15, 22*). A series of mutations were made to the Pro at L209 in one of these channels (*22, 23*). Crystal structures show that when Pro L209 is changed to Glu, the water chain is disrupted by the Glu carboxylate. In addition, unexpectedly, the mutation of L209 to Tyr causes the Q_B quinone to shift to the proximal position even in dark-adapted RC crystals (*24*). Thus, the different mutants in this series allow the importance of quinone position and water chain continuity for electron transfer from Q_A^- to Q_B to be tested.

MATERIALS AND METHODS

The reaction centers from the three L209 mutants were prepared as described in (*23*). The optical measurement and data analysis have been described previously (*11*). For quinone isoprenoid tail dependence measurements the His-tagged *Rhodobacter sphaeroides* strain (*25*) and ubiquinones UQ-1 (Sigma), UQ-4 (Fluka), and UQ-10 (Sigma) were used. The mutant RCs were also frozen under illumination in the light-adapted state, as described previously (*11*). All the measurements used ≈3−4 μM MRCs in 10 mM Tris buffer, pH 8.0, with 66% glycerol (v/v).

The rate of electron transfer from Q_A^- to Q_B (k_{AB}) was obtained from the quantum yield (Φ) for forming $P^+Q_B^-$. $P^+Q_A^-$ formed by the actinic flash goes on to $P^+Q_B^-$ (at k_{AB}) or back to the ground state (at k_{AP}). $P^+Q_B^-$ re-forms the ground state at a slower rate. Φ is determined from the

amplitudes of the slow (A_S) and fast (A_F) components of the P^+ charge recombination. Charge recombination from $P^+Q_B^-$ is slower (<1 s^{-1}) and from $P^+Q_A^-$ faster (~10 s^{-1}) (*11*). This method provides a good estimate for k_{AB} when it is comparable to k_{AP}. Thus:

$$\Phi = \frac{A_S}{A_S + A_F} = \frac{k_{AB}}{k_{AB} + k_{AP}} \qquad (1)$$

Given k_{AP}, Φ provides k_{AB}. k_{AP} has been extensively measured in wild-type RCs with no Q_B, where it is essentially temperature (*26, 27*) and pH (*28*) independent. At room temperature, k_{AP} is the same in the mutant and the wild-type protein. The analysis assumes this remains temperature-independent. In the samples used here, the RCs are 80−95% saturated with ubiquinone Q_B. The fraction which cannot form $P^+Q_B^-$ is determined at room temperature, where Φ is ≈1 and subtracted from A_F before Φ is calculated. This assumes the Q_B site occupancy is temperature-independent.

When directly measured, k_{AB} is not well-characterized as a single exponential (*9*). Inhomogeneous kinetics will introduce errors into the calculation of k_{AB} from Φ and into the derived activation parameters as described previously (*13*). If micro-states of $P^+Q_A^-$ with slower rates of electron transfer from Q_A^- to Q_B become increasingly important at low temperature, $\Delta H^{\ddagger}_{AB}$ and the rate extrapolated to infinite temperature will be too large.

In RCs, the equilibrium constant between $P^+Q_A^-$ and $P^+Q_B^-$ (K_{AB}) was determined in situ from the rate at which $P^+Q_B^-$ returns to the ground state (PQ_AQ_B) (k_{BP}^{obs}) using

$$k_{BP}^{obs} = k_{BP} + \frac{k_{AP}}{1 + K_{AB}} \qquad (2)$$

as described previously (*13, 28−30*). The temperature dependence of $\Delta G°_{AB}$ provides $\Delta H°_{AB}$ and $\Delta S°_{AB}$.

RESULTS

Effect of the Isoprenoid Tail on the Kinetics. At room temperature, the rate of electron transfer from Q_A^- to Q_B has been found to be independent of the length of the isoprenoid tail (*20, 21*). The temperature dependence of the Q_A^- to Q_B quantum efficiency (Φ) was determined as a function of the Q_B tail length (Figure 1). Q_B was reconstituted with the 5-carbon, 1-isoprene tail (UQ-1); the 20-carbon, 4-isoprene tail (UQ-4), and the native 10-isoprene tail (UQ-10). The decrease in Φ and therefore k_{AB} as the temperature is lowered is independent of the tail length. Thus, the bulky isoprene tail does not contribute to the barrier to electron transfer.

L209 Pro Mutants. The change in free energy of electron transfer was determined from the rate of the thermal back-reaction in the wild-type and Pro mutant RCs (eq 2). The temperature dependence of $\Delta G°_{AB}$ provides $\Delta H°_{AB}$ and $\Delta S°_{AB}$ (*13*). At room temperature, $\Delta G°_{AB}$ is 10−30 meV less favorable in the mutants. The Thr mutant has a more favorable $\Delta H°_{AB}$ and less favorable $\Delta S°_{AB}$ while the Tyr and Glu mutants change in the opposite direction. These changes fit the common pattern of entropy−enthalpy compensation. Stronger interactions are balanced by more constraints keeping $\Delta G°$ essentially constant.
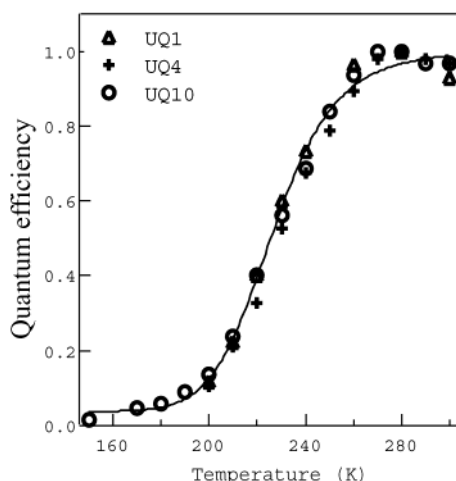
FIGURE 1: Temperature dependence of the quantum yield for Q_A^- to Q_B electron transfer in wild-type RCs with ubiquinone with different hydrocarbon tails. The electron-transfer rate (k_{AB}) is determined from Φ with eq 1. The uncertainty of Φ is $\pm 2\%$. The theoretical line assumes a single barrier for electron transfer with activation parameters given for the wild-type RCs in Table 1 (*13*).

Table 1: Equilibrium Free Energy, Enthalpy, and Entropy Changes between $P^+Q_A^-$ and $P^+Q_B^{-\ a}$

meV at 298 K	WT	L209 PY	L209 PT	L209PE
$\Delta G°_{AB}$	-90 ± 10	-80 ± 10	-80 ± 10	-60 ± 10
$\Delta H°_{AB}$	-230 ± 20	-180 ± 30	-380 ± 20	-120 ± 30
$-T\Delta S°_{AB}$	$-(-140 \pm 20)$	$-(-100 \pm 30)$	$-(-300 \pm 20)$	$-(-60 \pm 30)$
$*k_{AB}$ (s^{-1})	7875	5300	5350	6620

a Values derived from the temperature dependence of charge recombination from $P^+Q_B^-$ to the ground state via thermal repopulation of $P^+Q_A^-$ (see *13* for a complete description of the model and data analysis). $*k_{AB}$ from ref (*23*) was measured by monitoring the electrochromic shift accompanying the electron transfer at pH 8.1, 294 K.
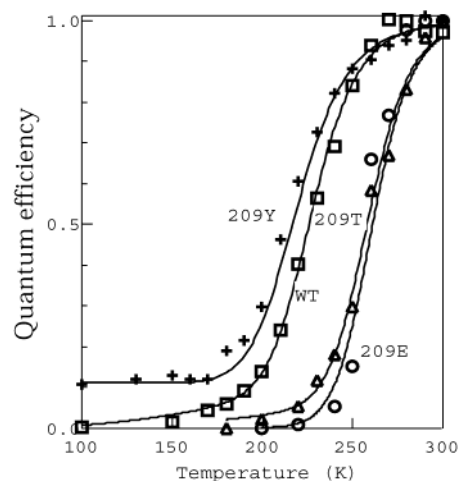

FIGURE 2: Temperature dependence of the quantum yield for wild-type RCs and the three L209 mutants. The model and parameters used to fit the data are described in Table 2.

Table 2: Activation Energy, Entropy, and Enthalpy for the Wild-Type RCs and L209 Mutants at pH 8.0^a

meV at 298 K	wild type	L209PY	L209PT	L209PE
$\Delta G^{\ddagger}_{AB}$	500 ± 100	540 ± 60	550 ± 70	520 ± 70
$\Delta H^{\ddagger}_{AB}$	420 ± 80	260 ± 40	500 ± 60	530 ± 60
$-T\Delta S^{\ddagger}_{AB}$	$-(-80 \pm 60)$	$-(-280 \pm 40)$	$-(-50 \pm 40)$	$-(10 \pm 40)$

a The yield of $P^+Q_B^-$ is obtained given a model where $P^+Q_A^-$ goes to $P^+Q_B^-$ (at k_{AB}) or to the ground state (at k_{AP}) and is formed from $P^+Q_B^-$ (k_{BA}). $P^+Q_B^-$ goes to $P^+Q_A^-$ (at k_{BA}) or the ground state (at k_{BP}) and is formed from $P^+Q_A^-$. Formation of the ground state is irreversible. All reactions are unimolecular. For wild-type RCs and for the Pro L209 to Tyr mutant, there is an activated substate, ≈ 40 meV above $P^+Q_A^-$, which forms $P^+Q_B^-$ essentially instantaneously. The $\Delta S°$ between the active and inactive $P^+Q_A^-$ substates is assumed to be 0 in wild-type RCs while $\Delta H° = 0$ in L209PY RCs (see ref *13* for a complete description of the model and data analysis).

The rate of electron transfer from Q_A^- to Q_B when Pro L209 was mutated to Tyr, Glu, and Thr was previously measured at 294 K, and the rates were found to vary by less than 30% (*23*) (Table 1). k_{AB} was determined as a function of temperature from the quantum yield for electron transfer. When wild-type RCs are frozen in the light in the $P^+Q_B^-$ state, the system returns to the ground redox state in a form where the required conformational changes are frozen in. Now Φ is 100% even at temperatures below 40 K (*10, 11*). The same behavior is found in the L209 mutants, showing the mutations do not affect the ability of the protein to be trapped in an active conformation at low temperature.

As in the native RCs in the dark-adapted protein, Φ decreases with temperature in all three mutants, indicating k_{AB} is slowing to be comparable to k_{AP} (Figure 2). When Pro L209 is replaced with Thr or Glu, Φ decreases to 50% at ~260 K, a significantly higher temperature than in wild-type RCs. The Glu mutant has the steeper temperature dependence of the two. However, when Pro is replaced with Tyr, the reaction freezes out at lower temperature than the wild-type RCs. In addition, below 240 K, Φ falls to zero more slowly in the L209PY than in wild-type protein, showing there is a small population that remains capable of forming product.

For L209PE and L209PT RCs, the theoretical lines in Figure 2 assume a single barrier between $P^+Q_A^-$ and $P^+Q_B^-$

with thermodynamic and activation parameters given in Table 2 [see (*13*) for a complete description of the kinetic model]. However, the slow fall of Φ to zero in L209PY RCs at low temperature cannot be accommodated by a model with a single barrier. Although less obvious, as seen before (*13*), Φ in wild-type RCs also falls more slowly to zero than predicted by the simplest model. Therefore, the lines through the wild-type and L209PY RCs assume a second $P^+Q_A^-$ substate capable of rapid electron transfer (*13, 21*). This substate would be similar to that found in the active, light-adapted RCs (*11*). The active state is estimated to be ≈ 40 meV above the relaxed reactant, and the two remain in equilibrium. In the wild-type RCs, assuming $\Delta G° = \Delta H°$ for the relaxed and activated substates provides a reasonable correspondence between experiment and simulation. In L209PY, the very long asymptote is incompatible with this model. Rather the simulation uses $\Delta G° = -T\Delta S°$, $\Delta H° = 0$. These parameters yield a good fit to Φ for the mutant in the temperature region shown, but they underestimate the $\Delta H°$ between active and inactive substates since Φ does go to zero in the L209PY RCs by 40 K.

At room temperature, the barrier to electron transfer is similar in wild-type RCs and the three mutants as seen by the similarity of reaction rate and $\Delta G°$ (Table 1). However, the change in the temperature dependence of Φ shows the nature of the barrier is different. In particular, the Tyr mutant

has a significantly smaller $\Delta H_{AB}^{\ddagger}$ and a larger $\Delta S_{AB}^{\ddagger}$. Thus, entropy-enthalpy compensation keeps $\Delta G_{AB}^{\ddagger}$ relatively constant at room temperature.

DISCUSSION

The electron transfer from Q_A^- to Q_B is not limited by the electron tunneling reaction itself, but is gated by unknown conformational changes. This has been established by the observation that the reaction rate is independent of the reaction driving force (*8, 21*). In RCs, when electron tunneling is rate-determining, the reaction shows a dependence on the driving force predicted by the Marcus electron-transfer theory (*21, 31–33*).

RCs can be prepared in different substates of the reactant $P^+Q_A^-$ with different rate-determining steps for electron transfer to Q_B. For example, when the driving force is increased in isolated RCs by replacing the ubiquinone at the Q_A site with lower potential quinones, a component of the reaction becomes limited by the electron transfer itself and not by the conformational gating step (*21*). At high pH, proton uptake becomes rate-limiting (*11*). In addition, when RCs are frozen in the light (in the $P^+Q_B^-$ state), the RCs carry out electron transfer from Q_A^- to Q_B rapidly, at high yield even at temperatures below 40 K (*10, 11*). Thus, light-adapted RCs return to the ground redox state trapped in a high-energy substate where the changes required for reaction are frozen in. The question is what differences between the light- and dark-adapted protein are essential for the electron transfer. It has been suggested that the motion of quinone from an outer, distal binding site to an inner, active proximal Q_B site is one critical change (*14*).

RC crystals prepared in the ground (dark-adapted) and $P^+Q_B^-$ (light-adapted) states show the quinone in different positions. The two sites are displaced by about 4 Å along the path of the isoprenoid tail, and the quinone ring planes differ by a 180° rotation around the tail. Molecular dynamics simulations suggest that the proximal site is preferred after changes in Q_B site residue protonation in response to reduction of Q_A (*17*). However, while quinone translation from distal to proximal sites happens readily in the simulation, there is a barrier to the needed ring flip within both binding sites and in the channel separating them (*34*).

If the translation and rotation of the quinone limits the electron-transfer rate, then fixing the quinone in the proximal site or changing the quinone tail length might be expected to change the height of the barrier for electron transfer. The electron-transfer rate at room temperature is independent of the quinone tail length (*20, 21*). The identical temperature dependence for RCs with UQ-1, UQ-4, and UQ-10 as Q_B shows that the bulky, 50 carbon, tail does not contribute to the reaction barrier. This could indicate that quinone movement is not rate-limiting. However, the barrier could still come from the need to break a hydrogen bond as the quinone leaves the proximal site or from protein distortions as the quinone headgroup rotates in the binding channel.

The importance of the motion of the quinone headgroup is tested in the L209 Pro to Tyr mutant, which is shown in crystal structures to be fixed in the proximal position even when prepared in the dark (*24*). Electron transfer slows with decreasing temperature in L209PY RCs, showing there is still a significant barrier to reaction. In contrast, when frozen

in light, the electron transfer proceeds with high quantum efficiency, demonstrating that these RCs can be trapped in a fully active conformation. The L209PY mutant does have a larger population of active substate than do wild-type RCs as shown by Φ being $\approx$5% at 100 K (Figure 2). Φ does go to 0 by 40 K (not shown). Thus, the mutation shifts the balance between $\Delta H°$ and $\Delta S°$ in the equilibrium between inactive and the higher energy, active, dark-adapted substates.

It is possible that differences between crystal and glycerol glass change the equilibrium distribution between distal and proximal sites in the L209PY RCs favoring distal binding here. The L209 mutant crystals were grown without cryo-protectant and the data collected at 5 °C (*24*). The limited, available evidence suggests that solvent composition does not strongly change the quinone position. The quinone remains in the distal site in frozen crystals of dark-adapted RCs grown with (*14*) and without (*15*) poly(ethylene glycol), a cryo-solvent that may resemble the glycerol used here. The distal to proximal transition in the light-adapted RC crystals occurs in the presence of poly(ethylene glycol) (*14*). Thus, if it is assumed that the quinone position is as found in the crystal, the slowing of k_{AB} with temperature shows motions other than quinone translation must be rate-limiting in the dark-adapted Tyr L209 mutant.

The RC crystal structure resolution is insufficient to show if the Tyr mutant has the same orientation of the quinone head found in the light-adapted crystals (*24*). It is therefore possible that the quinone ring flip remains rate-limiting in the mutant. However, molecular dynamics simulations suggest that the incorrectly oriented headgroup is unlikely to be found in the proximal site (*34*). Thus, if the quinone is properly oriented in the proximal site in the dark-adapted mutant RCs, the quinone movement does not appear to constitute the conformational gate for electron transfer.

The mutation of the L209 proline influences the equilibrium and activation enthalpy and entropy changes for the electron transfer from Q_A^- to Q_B. But at room temperature, the enthalpy and entropy changes largely cancel, keeping the free energy change from $P^+Q_A^-$ to $P^+Q_B^-$ or to the transition state almost unchanged. Entropy–enthalpy compensation is often found in biochemical studies, in general because stronger interactions lead to a more rigid structure with less conformational entropy. Theoretical analysis indicates that this is expected for systems with large fluctuations and high density of states (*35, 36*). It has been suggested that the often observed, apparently fortuitous cancellation of the entropy and enthalpy changes at room temperature is appropriate for intermolecular interaction of modest strength such as hydrogen bonds (*35*).

There are differences in the barrier for the electron transfer in wild-type and L209PY RCs. In wild-type protein, the room temperature $\Delta G_{AB}^{\ddagger}$ is predominantly enthalpic while in the mutant the barrier has a significant entropic component. This difference is seen in k_{AB} slowing at lower temperatures in mutant than wild-type RCs. In L209PE and L209PT, $\Delta H_{AB}^{\ddagger}$ is larger, so the rate falls off more rapidly with decreasing temperature. While there is no crystal structure for L209PT, the L209PE structure shows that the Glu carboxylate is inserted into the water chain. Thus, changes in water flexibility and connectivity may change the balance between $\Delta H_{AB}^{\ddagger}$ and $\Delta S_{AB}^{\ddagger}$.

REFERENCES

1. Genick, U. K., Borgstahl, G. E. O., Ng, K., Ren, Z., Pradervand, C., Burke, P. M., Srajer, V., Teng, T., Schildkamp, W., McRee, D. E., Moffat, K., and Getzoff, E. D. (1997) *Science 275*, 1471−1475.
2. Srajer, V., Teng, T., Ursby, T., Pradervand, C., Ren, Z., Adachi, S., Schildkamp, W., Bourgeois, D., Wulff, M., and Moffat, K. (1996) *Science 274*, 1726−1729.
3. Deng, H., Zhadin, N., and Callender, R. (2001) *Biochemistry 40*, 3767−3773.
4. Luecke, H., Schobert, B., Richter, H. T., Cartailler, J. P., and Lanyi, J. K. (1999) *Science 286*, 255−261.
5. Feher, G., Allen, J. P., Okamura, M. Y., and Rees, D. C. (1989) *Nature 339*, 111−116.
6. Gunner, M. R. (1991) *Curr. Top. Bioenerg. 16*, 319−367.
7. Blankenship, R. E., Madigan, M. T., and Bauer, C. E. (1995) *Anoxygenic Photosynthetic Bacteria*, Vol. 2, Kluwer Academic Publishers, Dordrecht, The Netherlands.
8. Graige, M. S., Feher, G., and Okamura, M. Y. (1998) *Proc. Natl. Acad. Sci. U.S.A. 95*, 11679−11684.
9. Li, J., Gilroy, D., Tiede, D. M., and Gunner, M. R. (1998) *Biochemistry 37*, 2818−2829.
10. Kleinfeld, D., Okamura, M. Y., and Feher, G. (1984) *Biochemistry 23*, 5780−5786.
11. Xu, Q., and Gunner, M. R. (2001) *Biochemistry 40*, 3232−3241.
12. Xu, Q., and Gunner, M. R. (2000) *J. Phys. Chem. B 104*, 8035−8043.
13. Xu, Q., and Gunner, M. R. (2002) *Biochemistry 41*, 2694−2701.
14. Stowell, M. H. B., McPhillips, T. M., Rees, D. C., Soltis, S. M., Abresch, E., and Feher, G. (1997) *Science 276*, 812−816.
15. Ermler, U., Fritzsch, G., Buchanan, S. K., and Michel, H. (1994) *Structure 2*, 925−936.
16. Lancaster, R., and Michel, H. (1997) *Structure 5*, 1339−1359.
17. Grafton, A. K., and Wheeler, R. A. (1999) *J. Phys. Chem 103*, 5380−5387.
18. Alexov, E., and Gunner, M. (1999) *Biochemistry 38*, 8253−8270.
19. Sham, Y. Y., Muegge, I., and Warshel, A. (1999) *Proteins: Struct., Funct., Genet. 36*, 484−500.
20. McComb, J. C., Stein, R. R., and Wraight, C. A. (1990) *Biochim. Biophys. Acta 1015*, 156−171.
21. Li, J., Takahashi, E., and Gunner, M. R. (2000) *Biochemistry 39*, 7445−7454.
22. Baciou, L., and Michel, H. (1995) *Biochemistry 34*, 7967−7972.
23. Tandori, J., Sebban, P., Michel, H., and Baciou, L. (1999) *Biochemistry 38*, 13179−13187.
24. Kuglstatter, A., Ermler, U., Michel, H., Baciou, L., and Fritzsch, G. (2001) *Biochemistry 40*, 4253−4260.
25. Goldsmith, J. O., and Boxer, S. G. (1996) *Biochim. Biophys. Acta 1276*, 171−175.
26. McElroy, J. D., Mauzerall, D. C., and Feher, G. (1974) *Biochim. Biophys. Acta 333*, 261−277.
27. Gunner, M. R., Robertson, D. E., and Dutton, P. L. (1986) *J. Phys. Chem. 90*, 3783−3795.
28. Kleinfeld, D., Okamura, M. Y., and Feher, G. (1984) *Biochim. Biophys. Acta 766*, 126−140.
29. Mancino, L. J., Dean, D. P., and Blankenship, R. E. (1984) *Biochim. Biophys. Acta 764*, 46−54.
30. Wraight, C. A., and Stein, R. R. (1980) *FEBS Lett. 113*, 73−77.
31. Gunner, M. R., and Dutton, P. L. (1989) *J. Am. Chem. Soc. 111*, 3400−3412.
32. Venturoli, G., Drepper, F., Williams, J. C., Allen, J. P., Lin, X., and Mathis, P. (1998) *Biophys. J. 74*, 3226−3240.
33. Allen, J. P., Williams, J. C., Graige, M., Paddock, M. L., Labahn, A., Feher, G., and Okamura, M. Y. (1998) *Photosynth. Res. 55*, 227−233.
34. Zachariae, U., and Lancaster, C. R. (2001) *Biochim. Biophys. Acta 1505*, 280−90.
35. Dunitz, J. D. (1995) *Chem. Biol. 2*, 709−712.
36. Qian, H., and Hopfield, J. J. (1996) *J. Chem. Phys. 105*, 9292−9298.

BI025573Y